

# INSIDE-OUT EVACUATION OF TRANSITIONAL PROTOPLANETARY DISKS BY THE MAGNETO-ROTATIONAL INSTABILITY

E. I. CHIANG<sup>1,2</sup> AND R. A. MURRAY-CLAY<sup>1</sup>

Accepted to Nature Physics June 7, 2007. This arXiv.org version contains more technical details and discussion.

## ABSTRACT

How do T Tauri disks accrete? The magneto-rotational instability (MRI) supplies one means, but protoplanetary disk gas is typically too poorly ionized to be magnetically active. Here we show that the MRI can, in fact, explain observed accretion rates for the sub-class of T Tauri disks known as transitional systems. Transitional disks are swept clean of dust inside rim radii of  $\sim 10$  AU. Stellar coronal X-rays ionize material in the disk rim, activating the MRI there. Gas flows from the rim to the star, at a rate limited by the depth to which X-rays ionize the rim wall. The wider the rim, the larger the surface area that the rim wall exposes to X-rays, and the greater the accretion rate. Interior to the rim, the MRI continues to transport gas; the MRI is sustained even at the disk midplane by super-keV X-rays that Compton scatter down from the disk surface. Accretion is therefore steady inside the rim. Blown out by radiation pressure, dust largely fails to accrete with gas. Contrary to what is usually assumed, ambipolar diffusion, not Ohmic dissipation, limits how much gas is MRI-active. We infer values for the transport parameter  $\alpha$  on the order of a percent for the prototypical systems GM Aur, TW Hyd, and DM Tau. Because the MRI can only afflict a finite radial column of gas at the rim, disk properties inside the rim are insensitive to those outside. Thus our picture provides one robust setting for planet-disk interaction: a protoplanet interior to the rim will interact with gas whose density, temperature, and transport properties are definite and decoupled from uncertain initial conditions. Our study also supplies half the answer to how disks dissipate: the inner disk drains from the inside out by the MRI, while the outer disk photoevaporates by stellar ultraviolet radiation.

*Subject headings:* accretion, accretion disks—X-rays: stars—stars: pre-main-sequence—solar system: formation—magnetohydrodynamics—planets and satellites: formation

## 1. INTRODUCTION: TRANSITIONAL DISKS AND THE MRI

Transitional disks surrounding pre-main-sequence, solar-type stars are identified by their spectral energy distributions (SEDs). At 1–10 microns wavelength, their excesses are weaker than those of classical, flat-spectrum T Tauri disks, while at longer wavelengths, their fluxes are as strong as those of any classical T Tauri SED. The deficit at infrared wavelengths is consistent with transitional disks having large inner “holes” that are fairly transparent in the continuum. Figure 1 illustrates the situation. Outside the hole radius  $a_{\text{rim}}$ , optically thick dust abounds. Inside  $a_{\text{rim}}$ , only trace amounts of optically thin dust are present.

Some of the more well-known transitional systems are listed in Table 1; these include GM Aur ( $a_{\text{rim}} \approx 24$  AU; Calvet et al. 2005, hereafter C05), TW Hyd ( $a_{\text{rim}} \approx 1$ –4 AU; Calvet et al. 2002, hereafter C02; Hughes et al. 2007; Ratzka et al. 2007), DM Tau ( $a_{\text{rim}} \approx 3$  AU; C05), and CoKu Tau/4 ( $a_{\text{rim}} \approx 10$  AU; D’Alessio et al. 2005). Interferometric measurements verify the existence of inner disk holes (Hughes et al. 2007; Ratzka et al. 2007; J. Brown, personal communication). Transitional disks may bridge the evolutionary gap between conventional T Tauri disks that do not have large inner clearings and debris disks that are entirely optically thin. Rim radii are too large to represent dust sublimation fronts, fu-

eling speculation that inside the hole, either (a) grains have grown too large for the medium to remain optically thick, (b) planets have consumed or torqued away material, and/or (c) the inner disk has drained onto the central star by accretion. This paper concerns possibility (c)—or more accurately, how accretion in transitional disks is ongoing.

Transitional disk holes are not empty. Though nearly devoid of dust, the region interior to  $a_{\text{rim}}$  often contains accreting gas. Near-ultraviolet excesses, when observed, imply stellar accretion rates of  $\dot{M} \sim 10^{-9} M_{\odot} \text{ yr}^{-1}$  (Muzerolle et al. 2000; C02; Bergin et al. 2004; C05); see Table 1. We seek here to explain the origin of such disk accretion. We propose that gas is leached from the inner disk rim by the magneto-rotational instability (MRI), a linear instability that amplifies magnetic fields in outwardly shearing disks and drives turbulence (Balbus & Hawley 1998). X-rays emitted by the hyperactive corona of the central star irradiate and ionize the disk rim, activating the MRI there. Magnetically active gas diffuses inward from the rim to the star. The inner hole grows as the MRI eats its way out. The accretion rate interior to the ever-expanding rim is steady (constant with radius) and entirely set by the accretion rate established at the rim.

Historically, whether the MRI is relevant to T Tauri disks has been a prospect fraught with doubt (see, e.g., Hartmann et al. 2006), as protoplanetary disk gas is typically too cold and/or too dusty to couple well to magnetic fields. The following two conditions must be met for the MRI to be viable. First, magnetic fields must be frozen

Electronic address: echiang@astro.berkeley.edu, rmurray@astro  
<sup>1</sup> Center for Integrative Planetary Sciences, Astronomy Department, University of California at Berkeley, Berkeley, CA 94720, USA

<sup>2</sup> Alfred P. Sloan Research Fellow

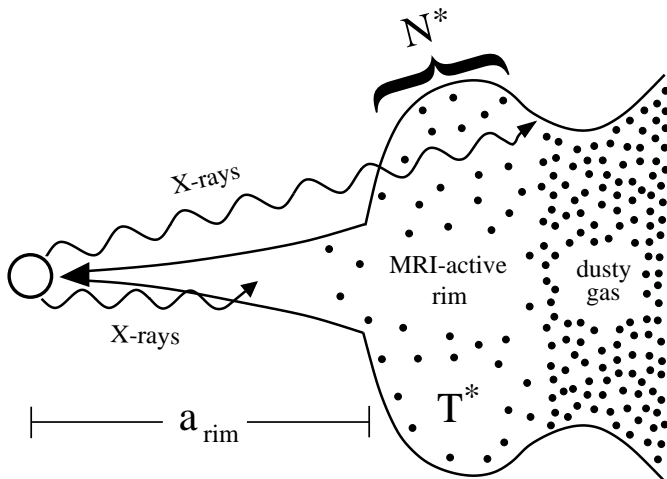


FIG. 1.— Schematic of a transitional protoplanetary disk accreting by the MRI. Transitional disks have large rims ( $a_{\text{rim}} \sim 10$  AU) inside of which dust is largely absent. Hard X-ray radiation from the young stellar corona photoionizes dusty rim gas and heats it to a temperature  $T^*$ . Only a limited gas column  $N^*$  is sufficiently ionized to be MRI-unstable and drain inwards. Stellar radiation pressure clears infalling gas of dust.

into whatever plasma is present. To freeze magnetic flux, the magnetic Reynolds number must be sufficiently large:

$$\text{Re} \equiv \frac{c_s h}{D} \approx 1 \left( \frac{a}{\text{AU}} \right)^{3/2} \left( \frac{T}{100 \text{ K}} \right)^{1/2} \left( \frac{x_e}{10^{-13}} \right) > \text{Re}^*. \quad (1)$$

Here we follow Fleming et al. (2000) in using the gas sound speed  $c_s$  and the vertical density scale height  $h = c_s/\Omega$  for characteristic velocity and length scales, respectively;  $\Omega$  is the Kepler orbital frequency;  $D$  is the magnetic diffusivity;  $T$  is the gas temperature;  $a$  is the disk radius; and  $x_e$  is the fractional electron density. Numerical simulations by Fleming et al. (2000) suggest  $\text{Re}^* \sim 10^2$ – $10^4$ , depending on the geometry of the seed field (but see Pessah, Chan, & Psaltis 2007 for a critical re-analysis of results related to the zero-net flux case; it is possible only the net vertical and net toroidal cases have their values of  $\text{Re}^* \sim 200$ – $3000$  well measured).

A second criterion—more often than not neglected in the protoplanetary disk literature—requires that neutral hydrogen molecules, constituting the bulk of disk matter, be dragged inward by accreting plasma (Blaes & Balbus 1994; Mac Low et al. 1995; Hawley & Stone 1998; Kunz & Balbus 2004). That is, ambipolar diffusion of the magnetized plasma out of the (overwhelmingly) neutral medium must not defeat the MRI. To couple the neutrals to the ions, a given  $\text{H}_2$  molecule needs to collide with enough ions within  $\sim 1/\Omega$ , the e-folding time of the instability:

$$\text{Am} \equiv \frac{x_e n \beta_{\text{in}}}{\Omega} > \text{Am}^*, \quad (2)$$

where  $\beta_{\text{in}} \approx 1.9 \times 10^{-9} \text{ cm}^3 \text{ s}^{-1}$  is the collisional rate coefficient for ions to share their momentum with neutrals (Draine, Roberge, & Dalgarno 1983) and  $n$  is the number density of hydrogen molecules (so that  $x_e n$  is the number density of ions). Linear growth rates for the MRI

drop dramatically with the degree to which criterion (2) is not satisfied (Kunz & Balbus 2004). The critical number  $\text{Am}^*$  of neutral-ion collisions is measured in numerical simulations to be about  $10^2$  (Mac Low et al. 1995; Hawley & Stone 1998). To our knowledge, these pioneering simulations have not been followed up or verified at higher resolution; therefore we regard this measurement of  $\text{Am}^*$ , like the measurement of  $\text{Re}^*$ , with caution. Criteria (1) and (2) are more easily met the more disk gas is ionized; criterion (1) depends on the fractional ionization, whereas (2) depends on the total ion density.

Transitional disks furnish an excellent first laboratory in which to investigate whether the MRI plays a role, if any, in how T Tauri disks accrete. Transitional disk holes are less plagued by sub-micron-sized dust that threatens to scour the region of plasma. Furthermore, the rim wall provides an especially simple geometry for analyzing how X-rays ionize disk material: if the wall is not severely shadowed from the star by material interior to the rim (see §5.2), one need only treat the 1-D radial transfer of radiation perpendicular to the rim wall.

X-ray driven MRI is not a new idea—it was originally introduced by Glassgold, Najita, & Igea (1997, hereafter GNI97)—but our study applies it for the first time to transitional disks and to identify the correct criterion for where the MRI can operate under these conditions. We argue that the entire region interior to the rim, including the midplane, is MRI-active. This contrasts with previous studies of X-ray driven (GNI97; Igea & Glassgold 1999, hereafter IG99) or cosmic-ray driven (Gammie 1996, hereafter G96; Sano et al. 2000) MRI in which accretion is confined to the surface layers of a disk whose midplane properties cannot be calculated from first principles. Moreover, such surface accretion is unsteady (G96). The accretion rates that we derive here are steady and can be directly compared to observations. Thus, transitional disks not only provide insight into the late stages of disk evolution, but also offer the first clean application of ideas—namely, MRI triggered by non-thermal ionization processes (G96; GNI97)—pioneered for more complex systems.

In §2, we construct a simple model for the rate of mass flow from the X-ray illuminated rim. We solve the equations of ionization and energy balance to decide how much of the rim satisfies criteria (1) and (2) and accretes. In addition to accounting for the usual dissociative recombination of molecular ions with free electrons (e.g., GNI97), our treatment of ionization balance includes recombination onto dust grains (Umebayashi & Nakano 1980) and charge transfer to free atomic metals (Oppenheimer & Dalgarno 1974, hereafter OD74; Fromang, Terquem, & Balbus 2002). We show how criterion (2), neglected in many studies of protoplanetary disks (e.g., G96; GNI97; IG99; Sano et al. 2000; Fromang et al. 2002; Matsumura & Pudritz 2003), supersedes criterion (1). We establish a relation between accretion rate  $\dot{M}$  and rim radius  $a_{\text{rim}}$  and compare to observations.

In §3, we demonstrate how the MRI continues to transport gas inward at radii  $a \ll a_{\text{rim}}$ . Though the midplane of the interior disk is optically thick to incident X-rays, Compton scattering permits enough X-rays to reach the midplane (IG99) that the MRI operates there as well. Accretion is therefore steady from the rim to the star.

In §4, we study in a preliminary way how stellar radiation pressure blows dust grains out of accreting gas and can keep the disk inside the rim relatively transparent. We make a connection to the small but non-zero optical depth inferred for the inner disk from SED modelling (C02; C05) to constrain the abundance of micron-sized grains in the rim.

Our work leaves many issues unresolved and calls attention to outstanding questions associated with the MRI. These are discussed in §5, after a summary of our principal findings.

## 2. ACCRETION FROM THE RIM

Ionization of rim gas is maintained by stellar X-rays.<sup>3</sup> As measured by *Chandra*, the X-ray spectra of T Tauri stars in Orion often have separate soft and hard components, modelled as emission from thermal plasmas having characteristic energies  $kT \approx 1$  keV and  $kT \approx 3$  keV, where  $k$  is Boltzmann's constant (Wolk et al. 2005, see their Figure 12). The luminosities of the two components are comparable, and depending on the star, range from  $10^{28}$  to  $10^{31}$  erg s<sup>-1</sup>. Soft, sub-keV X-rays are thought to be emitted by shock-heated gas in accretion columns (Kastner et al. 2002; Stelzer & Schmitt 2004), while hard, super-keV photons may arise from magnetic flares in stellar coronae (e.g., Wolk et al. 2005).

As the penetrating power of X-rays increases rapidly with photon energy, we are primarily interested in the hard, presumably coronal emission. Unfortunately, we are unable to locate detailed X-ray spectra at photon energies  $E_X \gtrsim 3$  keV for the prototypical transitional systems discussed in this paper (GM Aur, TW Hyd, DM Tau, and CoKu Tau/4). What we glean from the literature is summarized in Table 1. In the absence of detailed spectra, we assume for our computations below that each source emits  $L_X = 10^{29}$  erg s<sup>-1</sup> at a characteristic energy  $E_X = 3$  keV. This assumption is supported circumstantially by the aforementioned *Chandra* observations of hard X-ray emission from Orion pre-main-sequence stars. It is, furthermore, consistent with our findings in Table 1, even for TW Hyd, whose spectrum is known to be atypically soft (Stelzer & Schmitt 2004).

Stellar X-rays penetrate the exposed rim wall to a hydrogen column density  $N$  (see Figure 1). A limited column  $N^*$  will satisfy criteria (1) and (2). The MRI-active rim contains mass  $M_{\text{rim}} \approx 4\pi N^* a_{\text{rim}} h \mu$ , where  $h = c_s/\Omega$  is the vertical density scale height,  $c_s = (kT^*/\mu)^{1/2}$  is the gas sound speed,  $\Omega$  is the Kepler orbital frequency,  $T^*$  is the kinetic temperature of MRI-active gas at the rim, and  $\mu \approx 3 \times 10^{-24}$  g is the gas mean molecular weight. This mass flows from  $a_{\text{rim}}$  to  $\sim a_{\text{rim}}/2$  over the diffusion time  $t_{\text{diff}} \sim a_{\text{rim}}^2/\nu$ , where  $\nu = \alpha c_s h$  is the turbulent diffusivity:

$$\dot{M} \approx \frac{3M_{\text{rim}}}{t_{\text{diff}}} \approx \frac{12\pi\alpha N^* a_{\text{rim}}^2 (kT^*)^{3/2}}{GM_* \mu^{1/2}} \quad (3)$$

<sup>3</sup> Galactic cosmic rays at GeV energies yield ionization rates of at most  $\sim 10^{-17}$  s<sup>-1</sup> per H<sub>2</sub> (Spitzer 1978, p. 116). Actual cosmic ray ionization rates in T Tauri disks are likely much lower because of shielding by magnetized T Tauri winds. Even the much weaker solar wind modulates the cosmic ray flux at Earth by as much as  $\sim 10\%$  with solar cycle (Marsh & Svensmark 2003). We ignore cosmic ray ionization; it is easy to check that their contribution is negligible compared to ionization by stellar X-rays.

where  $G$  is the gravitational constant and the extra factor of 3 follows from a more accurate derivation (using  $\dot{M} = 3\pi\Sigma\nu$ , where  $\Sigma$  is the disk surface density; Frank, King, & Raine 1992). As measured by numerical simulations of the MRI, the transport parameter  $\alpha$  might be  $\sim 0.01$ – $0.3$ , depending on the strength and geometry of the background field (Fleming et al. 2000; Sano et al. 2004; Pessah et al. 2007; see also §5.2). Notice how  $\dot{M}$  in equation (3) does not depend explicitly on the surface density profile  $\Sigma(a)$  of the disk. Given observations of  $a_{\text{rim}}$  and  $M_*$ , one need only compute the rim-specific variables  $N^*$  and  $T^*$ , which we do below.

### 2.1. Ionization Balance

Determining  $N^*$  requires that we calculate the degree of ionization as a function of the radial column  $N$  penetrated by X-rays at the rim. Per H<sub>2</sub> molecule, the ionization rate is

$$\zeta = \frac{L_X}{4\pi a_{\text{rim}}^2 E_X} \eta \sigma_X \exp(-N\sigma_X) \quad (4)$$

where  $\sigma_X \approx 4 \times 10^{-24} (E_X/3 \text{ keV})^{-2.81} \text{ cm}^2$  is the photoionization cross-section per H<sub>2</sub> (assuming solar abundances) and  $\eta \approx 81$  accounts for the number of secondary ionizations produced per absorbed 3-keV photon (GNI97).

Freshly ionized H<sub>2</sub><sup>+</sup> rapidly converts to molecular ions such as HCO<sup>+</sup>. Most of these molecules dissociate in collisions with electrons, while some transfer their charge to gas-phase atomic metals such as magnesium (Fromang et al. 2002; OD74). The fractional number abundance  $x_{\text{mol}+}$  of molecular ions relative to neutral hydrogen molecules is given by the equilibrium relation

$$\zeta = x_{\text{mol}+} n (x_e \beta_{\text{diss}} + x_{\text{met}} \beta_t) \quad (5)$$

where  $\beta_{\text{diss}} \approx 3 \times 10^{-7} (T/230 \text{ K})^{-1/2} \text{ cm}^3 \text{ s}^{-1}$  and  $\beta_t \approx 10^{-9} \text{ cm}^3 \text{ s}^{-1}$  are rate coefficients for dissociation (Glassgold, Lucas, & Omont 1986) and charge transfer (OD74), and  $x_e$  and  $x_{\text{met}}$  are the fractional number densities of electrons and free neutral metals, respectively. To relate the number density  $n$  of neutral H<sub>2</sub> molecules to  $N$ , we spread all  $4\pi N a_{\text{rim}} h$  molecules comprising the X-ray penetrated rim into the volume  $2\pi a_{\text{rim}}^2 h$  interior to the rim to estimate that  $n \approx 2N/a_{\text{rim}}$ .

Charge transfer to free metals is important for sustaining the MRI because ionized metals tend to keep their charge, neutralizing slowly either by radiative recombination with electrons or collisions with negatively charged dust grains (OD74; Umebayashi & Nakano 1980; Glassgold et al. 1986):

$$x_{\text{mol}+} x_{\text{met}} \beta_t = x_{\text{met}+} (x_e \beta_{\text{rec}} + \beta_{\text{gr}}) \quad (6)$$

where  $x_{\text{met}+}$  is the fractional abundance of metal ions,  $\beta_{\text{rec}} \approx 4 \times 10^{-12} (T/230 \text{ K})^{-1/2} \text{ cm}^3 \text{ s}^{-1}$  is the radiative recombination coefficient, and  $\beta_{\text{gr}}$  is the recombination coefficient, measured per H<sub>2</sub>, for grains. We assume the total grain surface area available for recombination is dominated by grains of radius  $s$  containing a fraction  $Z_s$  of the total mass in gas and dust. It follows that  $\beta_{\text{gr}} \approx 3 \times 10^{-20} (\mu\text{m}/s) (Z_s/10^{-4}) (T/230 \text{ K})^{1/2} \text{ cm}^3 \text{ s}^{-1}$ .

TABLE 1  
PROPERTIES OF TRANSITIONAL DISK SYSTEMS

Star	$a_{\text{rim}}$ (AU)	$a_{\text{rim}}$ refs.	$\dot{M}$ ( $10^{-9} M_{\odot} \text{ yr}^{-1}$ )	$\dot{M}$ refs.	$L_{X,\text{obs}}^a$ ( $\text{erg s}^{-1}$ )	X-ray band observed (keV)	X-ray refs.
GM Aur	24	1	2.7–10	1,2	$10^{30}$	0.2–2.4	3
TW Hyd	$1\text{--}4^b$	4,5,6	0.3–0.7 <sup>c</sup>	4,7	$1.4 \times 10^{30}$	0.45–2.25	8
DM Tau	3	1	0.8–2	1,2	$2 \times 10^{29}$	0.3–10	9
CoKu Tau/4	10	10	< 0.1	11	NA	NA	12

REFERENCES. — 1. C05; 2. Bergin et al. 2004; 3. Strom et al. 1990; 4. C02; 5. Hughes et al. 2007; 6. Ratzka et al. 2007; 7. Muzerolle et al. 2000; 8. Stelzer & Schmitt 2004; 9. Guedel et al. 2007; 10. D’Alessio et al. 2005; 11. Najita et al. 2007; 12. König et al. 2001

<sup>a</sup> In modelling the hard X-ray spectrum incident upon the rim, we do not simply use the observed X-ray luminosity  $L_{X,\text{obs}}$ , which is typically measured for soft ( $E_X < 3 \text{ keV}$ ) photons having low penetrating power. Instead, we assume in our calculations of ionization and thermal balance that each star emits  $L_X = 10^{29} \text{ erg s}^{-1}$  at a characteristic photon energy  $E_X = 3 \text{ keV}$ .

<sup>b</sup> Controversy exists whether  $a_{\text{rim}} \approx 4 \text{ AU}$  (C02; Hughes et al. 2007) or is nearly  $\sim 1 \text{ AU}$  (Ratzka et al. 2007) for TW Hyd. For our analysis we adopt the former result, since it is based on methods similar to those applied for GM Aur, DM Tau, and CoKu Tau/4. The conclusions of our paper are unaffected by this choice.

<sup>c</sup> Taken to span a factor of 2 to reflect U-band variability (Muzerolle et al. 2000).

This estimate, which assumes that every grain is negatively charged, agrees with that of Umebayashi & Nakano (1980), who assume  $s \approx 0.1 \mu\text{m}$  and  $Z_s \approx 10^{-2}$ . Though unknown, the factor  $Z_s$  is likely to be considerably less than the maximal value permitted by solar abundance gas,  $Z_{\odot} \approx 10^{-2}$ , because of grain growth.<sup>4</sup> We take as standard values  $Z_s = 10^{-4}$  and  $s = 1 \mu\text{m}$ . A constraint on  $Z_s/s$  from observations is contained in §4 on radiation blow-out.

In assuming a single grain size, we neglect effects introduced by smaller-sized grains. The surface area for ion recombination may be dominated by very small grains. Furthermore, because grains efficiently adsorb electrons, they can, if sufficiently numerous, completely clear the gas of free electrons and catastrophically reduce the electrical conductivity. Indeed, this is the case in the Earth’s lower atmosphere, where charges are carried by aerosols. Fortunately, as we describe below in §2.3, our results enjoy some margin of safety from these effects. The fractional electron densities that we derive,  $10^{-7}\text{--}10^{-8}$  (compared, say, with terrestrial ionization fractions  $\sim 10^{-16}$  at sea level), are large enough that the chemistry is arguably driven by electrons (but see §5.2).

Charge and number conservation read, respectively,

$$x_e = x_{\text{mol}+} + x_{\text{met}+} \quad (7)$$

and

$$x_{\text{met,tot}} = x_{\text{met}+} + x_{\text{met}}. \quad (8)$$

Because free metals are depleted onto grains,  $x_{\text{met,tot}}$  is realistically at most  $\sim 3 \times 10^{-6}$ , corresponding to 1 out of every 10 metals in the free atomic phase (OD74; Umebayashi & Nakano 1980). We consider values for  $x_{\text{met,tot}}$  ranging from zero (complete depletion) up to  $10^{-6}$ .

We combine equations (5), (6), (7), and (8) to derive, under certain approximations, a quartic equation for  $x_e$  in terms of  $\zeta/n$ ,  $x_{\text{met,tot}}$ , and various rate coefficients.

<sup>4</sup> If grain growth were so extreme that an individual grain shielded itself from incident X-rays, then we would have to reduce the X-ray cross-section  $\sigma_X$  (which is measured per  $\text{H}_2$ ).

Equations (5), (6), and (7) yield

$$\beta_{\text{diss}} x_e^2 + \beta_t x_{\text{met}} x_e - \frac{\zeta}{n} - \frac{\zeta}{n} \left( \frac{x_{\text{met}} \beta_t}{x_e \beta_{\text{rec}} + \beta_{\text{gr}}} \right) = 0. \quad (9)$$

The first term on the left-hand side dominates the second term when

$$x_e \gg \frac{\beta_t}{\beta_{\text{diss}}} x_{\text{met,tot}} \approx 3 \times 10^{-9} \left( \frac{x_{\text{met,tot}}}{10^{-6}} \right) \left( \frac{T}{230 \text{ K}} \right)^{1/2}. \quad (10)$$

This is always the case for MRI-active rim material, as will be evident below (see Figures 2 and 3). Therefore we drop the second term in (9) to write

$$\beta_t x_{\text{met}} = \left( x_e^2 \frac{n \beta_{\text{diss}}}{\zeta} - 1 \right) (\beta_{\text{rec}} x_e + \beta_{\text{gr}}). \quad (11)$$

Combining equations (5), (6), and (8), we have

$$(\beta_{\text{diss}} x_e + \beta_t x_{\text{met}}) x_{\text{met,tot}} = x_{\text{met}} \left[ \beta_{\text{diss}} x_e + \beta_t x_{\text{met}} + \frac{\zeta}{n} \left( \frac{\beta_t}{\beta_{\text{rec}} x_e + \beta_{\text{gr}}} \right) \right], \quad (12)$$

which simplifies, according to the same approximation embodied in (10), to

$$\beta_{\text{diss}} x_{\text{met,tot}} x_e = x_{\text{met}} \left[ \beta_{\text{diss}} x_e + \frac{\zeta}{n} \left( \frac{\beta_t}{\beta_{\text{rec}} x_e + \beta_{\text{gr}}} \right) \right]. \quad (13)$$

We solve (13) for  $x_{\text{met}}$  and substitute into (11) to write

$$\begin{aligned} & \beta_{\text{diss}} \beta_{\text{rec}} x_e^4 + \beta_{\text{diss}} \beta_{\text{gr}} x_e^3 + \frac{\zeta}{n} (\beta_t - \beta_{\text{rec}}) x_e^2 \\ & - \frac{\zeta}{n} (\beta_{\text{gr}} + \beta_t x_{\text{met,tot}}) x_e - \left( \frac{\zeta}{n} \right)^2 \frac{\beta_t}{\beta_{\text{diss}}} = 0. \end{aligned} \quad (14)$$

It is safe to ignore  $\beta_{\text{rec}}$  in comparison to  $\beta_t$ , so that

$$\begin{aligned} & x_e^4 + \left( \frac{\beta_{\text{gr}}}{\beta_{\text{rec}}} \right) x_e^3 + \left( \frac{\zeta}{n \beta_{\text{diss}} \beta_{\text{rec}}} \right) x_e^2 \\ & - \left( \frac{\zeta}{n \beta_{\text{diss}} \beta_{\text{rec}}} \right) \left( \frac{\beta_{\text{gr}}}{\beta_t} + x_{\text{met,tot}} \right) x_e \\ & - \frac{\beta_t}{\beta_{\text{rec}}} \left( \frac{\zeta}{n \beta_{\text{diss}}} \right)^2 = 0. \end{aligned} \quad (15)$$

This final equation is a quartic and not a cubic (OD74) because we allow for the possibility that nearly all gas-phase atomic metals might be ionized, via equation (8).

### 2.2. Thermal Balance

Gas is heated by fast photoelectrons at a rate per  $\text{H}_2$  molecule of

$$\Gamma = \frac{L_X}{4\pi a_{\text{rim}}^2} f \sigma_X \exp(-N\sigma_X) \quad (16)$$

where  $f \approx 0.5$  is the fraction of X-ray energy deposited into heat (Glassgold, Najita, & Igea 2004). Gas cools by ro-vibrational transitions of CO at a rate per  $\text{H}_2$  molecule of

$$\Lambda = 3.3 \times 10^{-25} (T/\text{K})^{1/2} \frac{\exp(-4292 \text{ K}/T)}{1 - \exp(-3084 \text{ K}/T)} \times x_{\text{CO}} (n/\text{cm}^{-3}) \text{ erg s}^{-1} \quad (17)$$

(Glassgold et al. 2004, their equations C7–C8). Here  $x_{\text{CO}} \approx 10^{-4}$  is the fractional abundance of CO, whose level populations are assumed thermal. Other cooling channels—dust-gas collisions and Lyman  $\alpha$  emission from hydrogen—are less important and ignored. We replace  $n$  in (17) with our estimate  $2N/a_{\text{rim}}$  (see §2.1), set  $\Gamma = \Lambda$  in thermal balance, and solve for  $T$  as a function of  $N$ . This result is necessary for solving the quartic (15) for  $x_e$  because rate coefficients depend on  $T$ .

For our standard parameters for GM Aur ( $L_X = 10^{29} \text{ erg s}^{-1}$ ,  $E_X = 3 \text{ keV}$ ,  $a_{\text{rim}} = 24 \text{ AU}$ ), we find that  $T$  drops from about 340 to 200 K as  $N$  increases from  $10^{22}$  to  $10^{24} \text{ cm}^{-2}$ . Results for  $T$  are very similar for TW Hyd and DM Tau. The insensitivity to input parameters is due to the exponential sensitivity of the cooling rate  $\Lambda$  to  $T$ .

### 2.3. The Active Column and Resultant Accretion Rate

Taking the run of  $T$  with  $N$  from our simple model of thermal balance in §2.2, we solve the quartic (15) numerically. The solution  $x_e$  is displayed against  $N$  in Figure 2 for parameters appropriate to GM Aur, for various choices of  $x_{\text{met,tot}}$ . Evidently the presence of free atomic metals raises the ionization fraction by up to two orders of magnitude. Results for TW Hyd and DM Tau are similar to within factors of two.

From  $x_e(N)$  we compute  $\text{Am}(N)$ , as shown in Figure 3 for the case of GM Aur. If  $\text{Am} > \text{Am}^* = 100$  strictly determined the viability of the MRI, then we would equate  $N^*$  with the maximum value of  $N$  for which  $\text{Am} = 100$ . However, given uncertainties in the value of  $\text{Am}^*$  and in the sharpness of criterion (2) in predicting the non-linear, saturated outcome of the MRI, only an order-of-magnitude estimate for  $N^* \sim 5 \times 10^{23} \text{ cm}^{-2}$  (the value for which  $\text{Am}$  peaks) seems justifiable. We adopt this same value of  $N^*$  for TW Hyd and DM Tau, for which very similar results for  $\text{Am}(N)$  obtain. For  $N = N^* = 5 \times 10^{23} \text{ cm}^{-2}$ , we find from our thermal balance model that  $T = T^* \approx 230 \text{ K}$ .

The ionization fractions,  $x_e \sim 10^{-8}$ – $10^{-7}$ , corresponding to  $N \sim N^*$  are so large that magnetic Reynolds numbers,  $\text{Re} \sim 10^7$ – $10^8$ , far exceed the critical values,  $\text{Re}^* \sim 10^2$ – $10^4$ , seemingly required for magnetic flux freezing (Fleming et al. 2000). Therefore accretion by the MRI in transitional disks is limited by ambipolar diffusion, not by Ohmic dissipation.

Electron densities exceed grain densities by 8–9 orders of magnitude, for our standard  $Z_s = 10^{-4}$  and  $s = 1 \mu\text{m}$ . Our neglect of a population of aerosols which can scour the gas of electrons is arguably safe. The differential

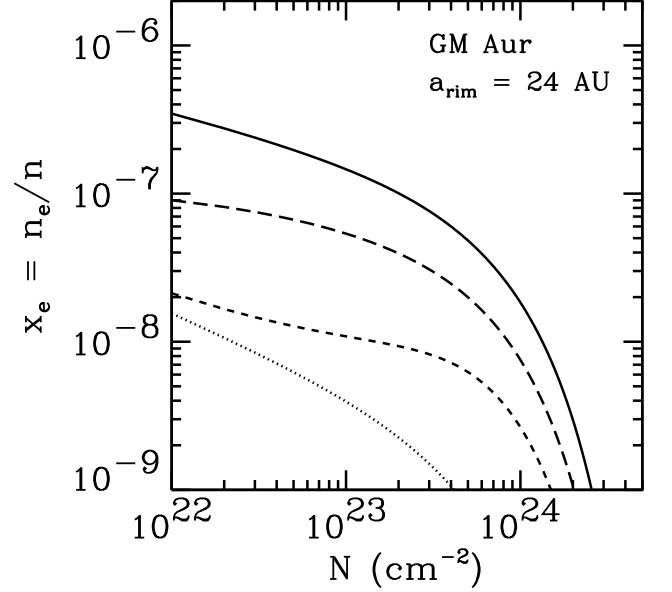


FIG. 2.— Ionization fraction  $x_e$  against column density  $N$  penetrated by X-rays at the rim, evaluated for GM Aur (assuming  $L_X = 10^{29} \text{ erg s}^{-1}$  and  $E_X = 3 \text{ keV}$ ). Curves are computed using the quartic equation (15) for  $x_e$ . Results for TW Hyd and DM Tau are similar. Solid, long-dashed, dashed, and dotted curves correspond to various choices for the gas-phase atomic metal abundance  $x_{\text{met,tot}}$ :  $10^{-6}$ ,  $10^{-7}$ ,  $10^{-8}$ , and 0, respectively. An abundance  $x_{\text{met,tot}} = 10^{-6}$  corresponds to 1 out of 30 metals in the atomic gas phase. Free atomic ions, which recombine slowly, can increase the ionization fraction by up to two orders of magnitude.

grain size distribution, if it scaled as  $s^{-3.5}$ , would have to extend from  $s = 1 \mu\text{m}$  all the way down to several angstroms for the total grain density to be comparable to the electron density. Our findings are also insensitive to the uncertain grain recombination coefficient  $\beta_{\text{gr}}$ , because metallic ions recombine more readily with electrons than with grains. For example, increasing  $\beta_{\text{gr}}$  by a factor of 30 above our nominal value (such an increase would correspond to the same grain size distribution mentioned above) decreases the peak value of  $\text{Am}$  in Figure 3 by a factor of 2, from 140 to 70.

Armed with  $N^*$  and  $T^*$ , we use equation (3) to plot  $\dot{M}$  against  $a_{\text{rim}}$  in Figure 4, adjusting  $\alpha$  as necessary to reproduce observed accretion rates for GM Aur, TW Hyd, and DM Tau. The offsets between the different lines drawn for different systems arise mostly from differences in  $M_*$  and  $\alpha$ , since  $N^* = 5 \times 10^{23} \text{ cm}^{-2}$  is held fixed and  $T^*(N^*, a_{\text{rim}})$  varies little. The slopes of the lines ( $\dot{M} \propto a_{\text{rim}}^2$ , approximately) reflect essentially the increase in the rim wall’s surface area with  $a_{\text{rim}}$ .

Best-fit  $\alpha$ ’s are 0.007–0.035. Such values are of order those seen in numerical simulations of the MRI, depending on the strength and geometry of the background field (Fleming et al. 2000; Sano et al. 2004; Pessah et al. 2007; see also §5.2).<sup>5</sup>

<sup>5</sup> Intriguingly, our best-fit  $\alpha$ ’s resemble those required to fit the light curves of dwarf novae during their “cold” states ( $\alpha \approx 0.02$ –

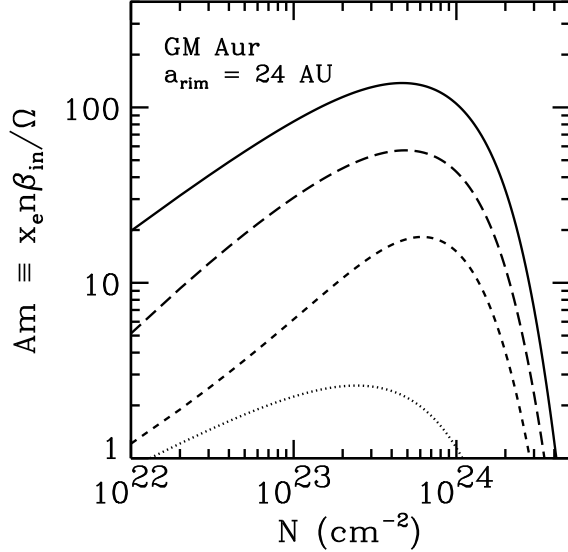


FIG. 3.— Ambipolar number  $Am$  against column density  $N$  penetrated by X-rays at the rim, evaluated for GM Aur (assuming  $L_X = 10^{29} \text{ erg s}^{-1}$  and  $E_X = 3 \text{ keV}$ ). Results for TW Hyd and DM Tau are similar. Solid, long-dashed, dashed, and dotted curves correspond to various choices for the free atomic metal abundance  $x_{\text{met,tot}}$ :  $10^{-6}$ ,  $10^{-7}$ ,  $10^{-8}$ , and 0, respectively. An abundance  $x_{\text{met,tot}} = 10^{-6}$  corresponds to 1 out of 30 metals in the atomic gas phase (i.e., 29 out of 30 depleted onto grains). The ambipolar numbers required for accreting plasma to entrain neutral hydrogen are measured in numerical simulations to be  $Am^* \sim 10^2$ . Roughly speaking,  $Am \sim Am^*$  for  $N = N^* \sim 5 \times 10^{23} \text{ cm}^{-2}$ , provided  $x_{\text{met,tot}} \gtrsim 10^{-7}$ .

The transitional system CoKu Tau/4 is not detected in X-rays (König et al. 2001) and has an unmeasurably small accretion rate ( $\dot{M} \lesssim 10^{-10} M_\odot \text{ yr}^{-1}$ ; Najita et al. 2007; D’Alessio et al. 2005), facts that at face value are consistent with our theory. Possibly CoKu Tau/4 has fewer free atomic metals or—and this is more readily testable—a softer X-ray spectrum than the other sources. If, say,  $Am \lesssim 10$  at its rim, then we estimate its 3-keV luminosity  $L_X \lesssim 10^{28} (10^{-8}/x_{\text{met,tot}}) \text{ erg s}^{-1}$ .

We expect little accreting material outside  $a_{\text{rim}}$ . The X-ray heated rim has a vertical thickness greater than that of material immediately outside. Thus, as depicted in Figure 1, some fraction of the disk beyond the rim will dwell in the rim’s X-ray shadow and be magnetically inert. Whatever distant material lies outside the rim’s shadow and might be accreting from X-ray irradiation is ignored. See also §5.1 for a reason to doubt that the outermost regions of disks accrete.

### 3. STEADY ACCRETION IN THE INTERIOR DISK

0.04; Lasota 2001). This resemblance seems sensible insofar as white dwarf accretion disks during their quiescent phases and protoplanetary disks both contain relatively cold, poorly ionized gas. However, Gammie & Menou (1998) argue that dwarf nova disks in quiescence do not support the MRI. These authors consider the relevant magnetic Reynolds numbers,  $Re \sim 3700$ , too low. Our own view is that such Reynolds numbers do not proscribe a weakened form of the MRI (see also Fleming et al. 2000).

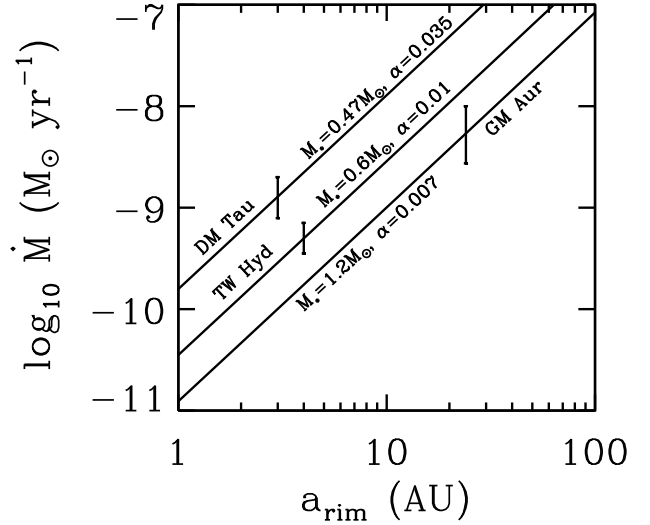


FIG. 4.— Accretion rates  $\dot{M}$  versus rim radii  $a_{\text{rim}}$ . Points with error bars represent observed data for GM Aur, TW Hyd, and DM Tau (see Table 1 for references). Solid lines are calculated according to equation (3), for  $N^* = 5 \times 10^{23} \text{ cm}^{-2}$ ,  $M_*$  as given by the literature for each star, and  $T^*$  as computed as a function of  $a_{\text{rim}}$  and  $M_*$  for fixed  $N^*$ . Offsets between lines mostly reflect differences in  $M_*$  and  $\alpha$ . The accretion rate  $\dot{M}$  increases with  $a_{\text{rim}}$ ; the larger the hole, the more surface area the rim wall exposes to X-rays. The transport parameter  $\alpha$  labelling each curve is chosen to reproduce the observations. Fitted values of  $\alpha$  range from 0.007 to 0.035, close to values reported in simulations of the MRI.

Once dislodged from the rim, gas must still travel up to three decades in radius, from  $\sim 10$  to  $\sim 0.01 \text{ AU}$ , to reach the stellar surface. We now argue that X-ray-driven MRI continues to provide transport at  $a \ll a_{\text{rim}}$ . At  $\sim 0.01 \text{ AU}$ , the MRI should be well sustained by thermal ionization. It remains to decide whether criteria (1) and (2) are satisfied at the midplane at radii of  $\sim 0.1$  to  $\sim 1 \text{ AU}$ . We need to estimate the temperature and surface density of material there.

Observed spectra demand that inside the rim, the disk contain so few grains as to be optically thin at mid-infrared wavelengths (C02; C05). We can understand this as a consequence both of the limited number of grains contained within the MRI-active mass  $M_{\text{rim}}$ , as well as stellar radiation pressure, which blows out a large fraction of grains having sizes  $s < 1 \mu\text{m}$  (see §4). Having lost its primary source of continuum opacity, the gas heats not by incident starlight, but by accretion (Ohmic dissipation). Cooling proceeds through line emission, at a rate that is difficult to estimate because it requires solving simultaneously for the thermal, chemical, and excitation state of the gas.

We do not attempt to construct a full-blown thermal model of electrically resistive, line-emitting gas. Instead, we find it adequate to estimate the temperature of midplane gas at  $a \ll a_{\text{rim}}$  in terms of its minimum possible value, obtained by equating the energy flux from accretion with that emitted by a blackbody:

$$T \approx 50 \left( \frac{\dot{M}}{10^{-9} M_{\odot} \text{ yr}^{-1}} \right)^{1/4} \left( \frac{a}{\text{AU}} \right)^{-3/4} \hat{T} \text{ K}, \quad (18)$$

where  $\hat{T} > 1$  parameterizes our uncertainty. Mass continuity then implies a vertical hydrogen column density of

$$N_{\perp} \approx 5 \times 10^{24} \left( \frac{\dot{M}}{10^{-9} M_{\odot} \text{ yr}^{-1}} \right)^{3/4} \left( \frac{a}{\text{AU}} \right)^{-3/4} \times \left( \frac{\alpha}{0.02} \right)^{-1} \hat{T}^{-1} \text{ cm}^{-2} \quad (19)$$

to the midplane. We have normalized  $\alpha$  to the average of values obtained for GM Aur, TW Hyd, and DM Tau (Figure 4).

Encouragingly, equation (19) yields surface densities that are entirely consistent with those inferred by Salyk et al. (2007) for GM Aur and TW Hyd: at  $a \sim 0.2$ – $0.5$  AU, these authors find  $N_{\perp} \sim 0.3$ – $3 \times 10^{24} \text{ cm}^{-2}$  ( $\text{H}_2$  surface densities of  $1$ – $10 \text{ g cm}^{-2}$  assuming  $x_{\text{CO}} = 2 \times 10^{-4}$ ), based on observations of rovibrational emission from CO. These same observations suggest that  $\hat{T} \approx 3$  (see their Figure 2), and we normalize our results below to this value.

To estimate Re and Am at the midplane, we first obtain the ionization rate  $\zeta$  from IG99, who calculate by Monte Carlo methods how X-rays incident upon disk surfaces propagate vertically and radially through protoplanetary disks. Their calculations account for multiple Compton scattering off bound electrons and for a thermal spectrum of photon energies. According to their Figure 3, for (a) a  $kT = 3 \text{ keV}$  plasma emitting  $L_X = 10^{29} \text{ erg s}^{-1}$ , (b)  $N_{\perp}$  as given by equation (19), and (c)  $\hat{T} = 3$ , the ionization rates at the midplane equal  $\zeta \approx 10^{-16} \text{ s}^{-1}$  at  $a = 1 \text{ AU}$  and  $\zeta \approx 2.5 \times 10^{-16} \text{ s}^{-1}$  at  $0.1 \text{ AU}$ .

We insert these rates into the quartic equation (15) for  $x_e$ , setting  $\beta_{\text{gr}} = 0$  because dust is largely absent in the inner disk. The quartic yields  $x_e \approx 2 \times 10^{-9}$  at  $1 \text{ AU}$  and  $x_e \approx 1 \times 10^{-9}$  at  $0.1 \text{ AU}$ , for  $x_{\text{met,tot}} = 10^{-6}$ . These ionization fractions correspond to  $\text{Re} \sim 2 \times 10^4$  at  $1 \text{ AU}$  and  $900$  at  $0.1 \text{ AU}$ , values that satisfy criterion (1), albeit marginally. Finally, taking  $n = N_{\perp}/h = N_{\perp}\Omega/c_s$ , we find that  $\text{Am} \approx 90$  at  $1 \text{ AU}$  and  $\text{Am} \approx 120$  at  $0.1 \text{ AU}$ . These values for Am, which marginally satisfy criterion (2), are insensitive to variations in  $\hat{T}$ , which produce changes in  $n$  that nearly cancel changes in  $x_e$ . The margins of safety for Re and Am would increase by accounting for thermal ionization.

We conclude that the MRI plausibly operates everywhere interior to the rim, even at the disk midplane, carrying steadily inward all of the mass drawn from the rim. Note how the MRI-active vertical columns at  $0.1$ – $1 \text{ AU}$ ,  $N_{\perp} \sim 10^{25} \text{ cm}^{-2}$ , are larger than the MRI-active radial column at the rim,  $N^* \sim 5 \times 10^{23} \text{ cm}^{-2}$ . This follows from criterion (2), which assigns importance to the total density  $x_e n$ , not the fractional density  $x_e$ . Total densities increase dramatically from the rim to the star.

#### 4. RADIATION BLOW-OUT OF GRAINS

Gas drawn from the rim entrains dust grains. As the surface density of inspiralling gas increases towards the

star, so, too, does the surface density of grains. Left unchecked, the increasing concentration of grains would render the inner disk optically thick at infrared wavelengths, violating observations. Here we explore how stellar radiation pressure can purge grains from gas (see also Eisner, Chiang, & Hillenbrand 2006).

Sub-micron-sized grains around solar-type stars feel an outward stellar radiation force that just exceeds stellar gravity. Then the time for such grains to travel from  $a$  to  $\sim 2a$  is

$$t_{\text{blow}} \sim \frac{1}{\Omega} \left( \frac{1/\Omega}{t_{\text{stop}}} \right) \quad (20)$$

where  $t_{\text{stop}} \sim \rho_p s / (c_s \mu n) < 1/\Omega$  is the time for grains of radius  $s$  and internal density  $\rho_p \approx 1 \text{ g cm}^{-3}$  to attain terminal velocity according to the Epstein gas drag law, which applies here because the grain size is smaller than the collisional mean free path in gas (e.g., Weidenschilling 1977). Radiation blow-out is faster than aerodynamic drift (the latter caused by radial pressure gradients in gas; e.g., Alexander & Armitage 2007) by  $(a/h)_{\text{rim}}^2 \sim 10^2$ , and so we ignore the latter.

We compare  $t_{\text{blow}}$  to  $t_{\text{diff}} \sim a^2/\nu$ , the time for gas to diffuse from  $a$  to  $\sim a/2$ . At the rim of the disk of GM Aur, the timescales match by coincidence:  $t_{\text{blow,rim}} \sim t_{\text{diff,rim}} \sim 1 \times 10^5 \text{ yr}$ . This indicates that about half of the dust in  $M_{\text{rim}}$  is expelled, leaving the other half entrained with accreting gas and spread between  $a_{\text{rim}}$  and  $\sim a_{\text{rim}}/2$ . The geometric optical depth of entrained dust, measured perpendicular to the midplane, is

$$\tau_{\text{rim}} \approx \frac{2N^* \mu Z_s}{\rho_p s} \frac{h}{a} \bigg|_{\text{rim}} \sim 0.5 \left( \frac{Z_s}{10^{-4}} \right) \left( \frac{\mu \text{m}}{s} \right). \quad (21)$$

We can try to check our estimate for  $\tau_{\text{rim}}$  against observations of the mid-infrared SED. Because radiation at a wavelength of  $10 \mu\text{m}$  originates from grains having temperatures of  $\sim 300 \text{ K}$ , observed  $10 \mu\text{m}$  spectra of GM Aur constrain the optical depth in grains at  $\sim 1 \text{ AU}$  but not near the rim at  $24 \text{ AU}$ , where starlight-heated grains would have colder temperatures of  $\sim 100 \text{ K}$ .<sup>6</sup> Therefore we cannot directly compare our calculated  $\tau_{\text{rim}}$  with  $10 \mu\text{m}$  observations for GM Aur.

For the case of TW Hyd, however, we can more easily make this comparison, because its rim is located at  $\sim 4 \text{ AU}$ . Scaling to the parameters of that system, we find  $t_{\text{blow,rim}} \sim 5 \times 10^3 \text{ yr}$  and  $t_{\text{diff,rim}} \sim 2 \times 10^4 \text{ yr}$ , which suggests that somewhat more than half of the dust in  $M_{\text{rim}}$  is expelled. Reducing our estimate in (21) by an additional factor of 2, and accounting for the smaller aspect ratio  $(h/a)_{\text{rim}}$ , we estimate  $\tau_{\text{rim}} \sim 0.1$  for TW Hyd. Observationally, the vertical optical depth of dust interior to the rim of TW Hydra's disk is  $\tau_{10} \approx 0.05$  at a wavelength of  $10 \mu\text{m}$  (C02). This is essentially the same as the geometric optical depth for micron-sized grains because of the silicate resonance band at  $10 \mu\text{m}$  wavelength. Thus, our crude estimate of  $\tau_{\text{rim}} \sim 0.1$ , based on assumed values for  $Z_s = 10^{-4}$  and  $s = 1 \mu\text{m}$ , is within a factor of two of the observed optical depth. Such approximate agreement we consider acceptable, and helps to justify our choice earlier for  $Z_s/s$  in calculating the grain recombination coefficient  $\beta_{\text{gr}}$  (§2.1).

<sup>6</sup> X-ray heated gas and starlight-heated grains generally have different temperatures.

To satisfy the observation that the disk remain optically thin at  $a \ll a_{\text{rim}}$ , the order-half of rim dust that lies between  $a_{\text{rim}}$  and  $a_{\text{rim}}/2$  must fail to penetrate inside  $a < a_{\text{rim}}/2$ . Radiation pressure ensures that dust does not continue to inspiral, provided that  $t_{\text{blow}}/t_{\text{diff}} \propto nT^{3/2}a^{5/2}$  decrease with decreasing  $a$ . This seems likely to obtain because  $T$  should drop sharply just inside  $a_{\text{rim}}/2$  once midplane gas becomes too dense to be heated effectively by X-rays. Unfortunately, a conclusive statement cannot be made without constructing a model that smoothly bridges conditions at  $a \sim a_{\text{rim}}$  with conditions at  $a \ll a_{\text{rim}}$ . This would require knowing in detail how gas heats and cools at all radii.

## 5. CONCLUDING REMARKS

We summarize our results in §5.1 and discuss topics for future research in §5.2.

### 5.1. Summary

How do T Tauri disks accrete? We have answered this longstanding question for the sub-class of objects known as transitional systems, disks having AU-sized or larger inner holes cleared of dust. Super-keV X-rays, emitted by the young star as a consequence of its enhanced dynamo, irradiate the inner disk rim. A portion of the rim is sufficiently ionized that it becomes unstable to the magneto-rotational instability (MRI) and diffuses inward. The MRI, sustained even at the disk midplane by hard X-rays, transports gas steadily from the rim all the way to the stellar surface. We infer transport parameters  $\alpha$  on the order of a percent; such values are indeed yielded by the MRI, according to contemporary numerical simulations.

We feel the following features of our theory deserve emphasis.

1. *Accretion rate vs. hole size.* All other factors (e.g., X-ray luminosity, stellar mass, free atomic metal abundance) being equal, the accretion rate  $\dot{M}$  should increase nearly as the square of the rim radius  $a_{\text{rim}}$ , simply from the increased surface area of the rim wall that is exposed to stellar X-rays. Late-breaking data (C. Espaillat, personal communication) for the transitional disks CS Cha ( $\dot{M} \approx 1.2 \times 10^{-8} M_{\odot} \text{ yr}^{-1}$ ,  $a_{\text{rim}} \approx 43 \text{ AU}$ ) and SZ 18 ( $\dot{M} \approx 1.7 \times 10^{-9} M_{\odot} \text{ yr}^{-1}$ ,  $a_{\text{rim}} \approx 14 \text{ AU}$ ) appear to support this trend of  $\dot{M}$  with  $a_{\text{rim}}$  as plotted in our Figure 4. Of course, this trend is expected to apply only for transitional disks for which  $a_{\text{rim}} \gtrsim 1 \text{ AU}$  (see the last issue raised in §5.2).
2. *Ambipolar diffusion vs. Ohmic dissipation.* Often it is assumed that Ohmic dissipation controls where the MRI can and cannot operate. This criterion, embodied in equation (1) through the magnetic Reynolds number  $\text{Re}$ , assigns importance to  $x_e$ , the ratio of the density of the most mobile charge carriers (electrons) to that of resistive species (neutral  $\text{H}_2$  molecules). Large values of  $\text{Re} \propto x_e$  imply that magnetic flux is frozen into plasma, enabling the background shear flow to amplify magnetic fields.

We have shown instead that ambipolar diffusion, not Ohmic dissipation, dictates the boundaries of

MRI-active zones. Magnetic flux can be perfectly frozen into plasma; yet if the neutrals do not couple mechanically to the plasma, the neutrals would be immune to the MRI. Protoplanetary disk gas is overwhelmingly neutral. Thus, as equation (2) states, a given neutral  $\text{H}_2$  molecule must collide with as many (momentum-bearing) ions as possible within a dynamical time for the MRI to afflict protoplanetary disk gas. Ambipolar diffusion limits the accretion flow from the rim, and is only marginally defeated at the midplane far inside the rim.

While we have demonstrated that criterion (2) outweighs (1) only for transitional disks, we suspect the same conclusion holds for conventional T Tauri disks as well. For example, consider Figure 7 of IG99, which seeks to describe the depth of the MRI-active layer in disks without holes. At, say,  $a = 1 \text{ AU}$ , at the bottom of the supposedly active layer of their model, the number density is  $n \sim N_{\perp}/h \sim 2 \times 10^{13} \text{ cm}^{-3}$ . By IG99's equation (23), the ionization fraction there is  $x_e \sim 4 \times 10^{-14}$  (for their standard  $\alpha = 1$ ). It follows that  $\text{Am} = x_e n \beta_{\text{in}} / \Omega \sim 10^{-2}$ . This falls four orders of magnitude short of the critical  $\text{Am}^* \sim 10^2$  seemingly demanded by numerical simulations (Mac Low et al. 1995; Hawley & Stone 1998). Therefore we disagree with IG99's determination of the depth of the active layer; their layer does not satisfy criterion (2).

Because the ambipolar diffusion criterion (2) assigns importance to the total ion density rather than the fractional electron density, it is hardest to satisfy in the most rarefied regions of disks, either at large vertical heights or large radial distance. This is just opposite to what has been concluded in the literature, that MRI-active zones are restricted to the surfaces and the outermost portions of disks.

3. *Robustness.* Disk properties inside the rim are insensitive to those outside, since the MRI can only draw a radial column of  $N^* \sim 5 \times 10^{23} \text{ cm}^{-2}$  from the rim at any time. In other words, unlike the usual situation, estimating  $\dot{M}$  does not require specifying the detailed surface density profile of the disk  $\Sigma(a)$ ; we need only know those rim-specific variables in equation (3):  $a_{\text{rim}}$ ,  $\alpha$ ,  $N_*$ , and  $T_*$ . Our picture therefore provides a robust setting for theories of how planets form and how their orbits evolve (e.g., Goldreich & Sari 2003) within transitional disks. A protoplanet lying interior to the rim will interact with gas whose density, temperature, and transport properties are definite and decoupled from uncertain initial conditions.
4. *How disks dissipate.* Our study also supplies part of the answer to how disks dissipate. Excepting matter that gets locked into planets, the inner disk drains from the inside out by the MRI, while material beyond the rim photoevaporates by stellar ultraviolet radiation (Alexander, Clarke, & Pringle 2006ab). Indeed, the models of Alexander et al. (2006ab) require the disk inside a few



AUs to drain onto the star before ultraviolet radiation can photoevaporate the outer disk efficiently. Their analysis did not specify the means by which the inner disk evacuates. Our work identifies the mechanism: it is the MRI, leaching material from the disk rim and causing the inner hole to grow. How long the MRI takes to eat its way out depends on the unknown surface density  $\Sigma$  of the original disk. The clearing time  $t_{\text{clear}} \sim \Sigma a_{\text{rim}}^2 / \dot{M} \sim 10^6$  yr if  $\Sigma \sim 10^2 \text{ g cm}^{-2}$  at  $a_{\text{rim}} \sim 10$  AU, comparable to that of the minimum-mass solar nebula.

### 5.2. Unresolved Issues

Numerous areas exist for improvement.

1. *Radiation blow-out.* We have established that a fraction on the order of 50% of the sub-micron-sized grains in the MRI-active rim gets blown back into the rim by stellar radiation pressure. The remaining fraction, which gets entrained to  $\sim a_{\text{rim}}/2$  by the accretion flow, ultimately must also be blown back to ensure that transitional disk holes stay as transparent as observed. To prove this last point requires understanding in detail how gas heats and cools at all radii from  $a_{\text{rim}}$  to the stellar surface, and checking that  $t_{\text{blow}}/t_{\text{diff}} \propto nT^{3/2}a^{5/2}$  decreases with decreasing  $a$ .

2. *Self-shadowing.* Throughout this work we have assumed for simplicity that the accretion disk interior to the rim does not obstruct the rim wall from stellar X-rays. Yet there must be some self-shadowing, which if sufficiently severe will convert the problem we have solved to one involving surface irradiation and the two-dimensional radiative transfer of X-rays (IG99). Even if this were the case, however, midplane gas at the rim may still be MRI-active by virtue of X-rays that Compton scatter downward from the disk surface (IG99; §3).

The rim might be tall enough that a good fraction of its lowermost vertical scale height escapes being shadowed. In our picture, rim gas is optically thin to X-rays, and is therefore well-heated by them (see also Glassgold et al. 2004). This source of heating is not enjoyed by midplane gas in the inner disk, which is optically thick to X-rays. Thus we envision a sharp drop in temperature and a concomitant drop in disk thickness just inside the rim. As was the case for radiation blow-out, addressing the problem of self-shadowing requires a global treatment of thermal balance.

3. *The value of  $\alpha$ .* We have estimated that  $\alpha$ 's on the order of a percent are required to explain the accretion rates of GM Aur, TW Hyd, and DM Tau. Such values are observed in numerical simulations of the MRI under certain assumptions about the magnitude and geometry of the seed magnetic field. Are these assumptions justified? What sets the seed field parameters? And how far can one trust the simulations themselves?

Using vertically unstratified simulations performed by Sano et al. (2004), Pessah et al. (2007) provide

a remarkably simple fitting formula for  $\alpha$ , which states that its saturation value scales as the background  $B_z/\sqrt{P}$ , where  $B_z$  is the mean strength of an assumed vertical magnetic field,  $P$  is the time-averaged gas pressure, and the simulation box length  $L$  is set equal to the pressure scale height  $h$ . Values of  $\alpha \sim 0.01$  correspond to  $B_z/\sqrt{P} \sim 0.008$ , or equivalently a plasma  $\beta \equiv 8\pi P/B_z^2 \sim 4 \times 10^5$ . Is such a background state realistic? Can one determine analogous requirements based on simulations that assume a net toroidal field, and ultimately on simulations that include vertical gravity?

4. *The value of  $\text{Am}^*$ .* Is  $\text{Am}^*$  truly and exactly 100? What is the origin of this dimensionless number? How sharp is criterion (2) in predicting the non-linear outcome of the MRI? According to our present calculations, criterion (2) for  $\text{Am}^* \sim 10^2$  is only marginally satisfied at the rim and interior to the rim. We need to know the transport parameter  $\alpha$  as a function of  $\text{Am}$  (see also point 3 above) to calculate more precisely the rate of gas flow from the rim.
5. *The value of  $x_{\text{met,tot}}$ .* How can one measure the abundance of gas-phase atomic metals in transitional disks? Our finding that the MRI is viable depends on having more than 1 out of every  $\sim 300$  metal atoms such as magnesium remaining in the atomic gas phase. These free metals provide the ions that collisionally couple the neutrals to the MRI.
6. *Aerosols.* What is the abundance of macromolecules/grains having sizes  $\sim 10\text{\AA}$  to  $\sim 0.1\mu\text{m}$  and is it large enough to interfere with the standard electron-driven chemistry we have presented? On the optimistic side, transitional disks are observed to have much less micron-sized dust than conventional T Tauri disks. We have calculated that fractional electron densities in the rim are large enough to withstand, to some degree, the effects of electron adsorption and ion recombination onto grains. On the other hand, radiation pressure cannot purge gas of small aerosols because of their short aerodynamic stopping times and low efficiencies for intercepting radiation.
7. *Accretion rate vs. X-ray luminosity.* Any mature theory of X-ray-driven MRI should predict  $\dot{M}$  as a function of  $L_X$ . But without knowing  $\alpha(\text{Am})$  (see points 3 and 4 above), we cannot derive this relation with confidence. At the very least  $\dot{M}$  must increase with  $L_X$ . Is there observational evidence for such a trend? In fact,  $\dot{M}$  is known to increase with  $M_*$  (e.g., Hartmann et al. 2006). And  $L_X$  is observed to increase with  $M_*$  (Guedel et al. 2007; Telleschi et al. 2007). But frustratingly enough, when  $\dot{M}$  is plotted against  $L_X$ , whatever trend might be present is obscured by large scatter (Telleschi et al. 2007).

A shorter-term project would be to measure the hard,  $E_X \gtrsim 3\text{ keV}$  spectra of individual sources.

The penetration depth of X-rays scales strongly with photon energy, as  $E_X^{2.81}$ .

8. *From conventional T Tauri disks to transitional disks.* We have studied the equilibrium dynamics of transitional disks but have said little regarding origin. Presumably transitional disks evolve from conventional T Tauri disks. Are transitional systems, as a group, older? The age of TW Hyd is estimated to be approximately 10 Myr, which indeed is old for a T Tauri star.

How does the evolution from conventional T Tauri to transition system take place? Unfortunately, we cannot answer this question by merely extrapolating our theory to earlier times. Our theory is designed to explain systems with large, well-defined holes, and would break down as  $a_{\text{rim}}$  approaches the stellar radius, if only because rim gas would be ionized thermally rather than by X-rays. Data for conventional T Tauri disks clearly do not fit the relations plotted in Figure 4; their rim radii

are on the order of  $\sim 0.1$  AU but their accretion rates range up to  $\sim 10^{-7} M_{\odot} \text{ yr}^{-1}$ . The origin of transitional disks will likely remain a mystery until we solve the decades-old puzzle of how conventional T Tauri disks, objects without large holes, accrete (see, e.g., Hartmann et al. 2006). The solution might involve some combination of the MRI plus gravitational instability (e.g., G96).

We thank Al Glassgold, David Hollenbach, Uma Gorti, Eric Feigelson, Martin Pessah, Catherine Espaillet, Joanna Brown, and Colette Salyk for informative discussions. Steve Balbus and an anonymous referee provided extensive and insightful criticisms that greatly improved the content of our manuscript. This work was motivated by lectures prepared by one of us (EIC) for the Hebrew University Winter School for Theoretical Physics, and supported by grants from the National Science Foundation and the Alfred P. Sloan Foundation.

#### REFERENCES

- Alexander, R.D., & Armitage, P.J. 2007, MNRAS, 375, 500  
 Alexander, R.D., Clarke, C.J., & Pringle, J.E. 2006a, MNRAS, 369, 216  
 Alexander, R.D., Clarke, C.J., & Pringle, J.E. 2006b, MNRAS, 369, 229  
 Balbus, S.A., & Hawley, J.F. 1998, Rev. Mod. Phys., 70, 1  
 Bergin, E., et al. 2004, ApJ, 614, 133  
 Blaes, O.M., & Balbus, S.A. 1994, ApJ, 421, 163  
 Calvet, N., et al. 2002, ApJ, 568, 1008 (C02)  
 Calvet, N., et al. 2005, ApJ, 630, 185 (C05)  
 D'Alessio, P., et al. 2005, ApJ, 621, 461  
 Draine, B.T., Roberge, W.G., & Dalgarno, A. 1983, ApJ, 264, 485  
 Eisner, J.A., Chiang, E.I., & Hillenbrand, L.A. 2006, ApJ, 637, 133  
 Fleming, T.P., Stone, J.M., & Hawley, J.F. 2000, ApJ, 530, 464  
 Frank, J., King, A., & Raine, D. 1992, Accretion Power in Astrophysics, Cambridge University Press  
 Fromang, S., Terquem, C., & Balbus, S.A. 2002, MNRAS, 329, 18  
 Gammie, C.F. 1996, ApJ, 457, 355 (G96)  
 Gammie, C.F., & Menou, K. 1998, ApJL, L75  
 Glassgold, A.E., Lucas, R., & Omont, A. 1986, A&A, 157, 35  
 Glassgold, A.E., Najita, J., & Igea, J. 1997, ApJ, 480, 344 (GNI97)  
 Glassgold, A.E., Najita, J., & Igea, J. 2004, ApJ, 615, 972  
 Goldreich, P., & Sari, R. 2003, ApJ, 585, 1024  
 Guedel, M., et al. 2007, A&A, in press (astro-ph/0609160)  
 Hartmann, L., D'Alessio, P., Calvet, N., & Muzerolle, J. 2006, ApJ, 648, 484  
 Hawley, J.F., & Stone, J.M. 1998, ApJ, 501, 758  
 Hughes, A.M., et al. 2007, ApJ, in press (arXiv:0704.2422)  
 Igea, J., & Glassgold, A.E. 1999, ApJ, 518, 848 (IG99)  
 Kastner, J.H., et al. 2002, ApJ, 567, 434  
 König, B., Neuhauser, R., & Stelzer, B. 2001, A&A, 369, 971  
 Kunz, M.W., & Balbus, S.A. 2004, MNRAS, 348, 355  
 Lasota, J.-P. 2001, New Astronomy, 45, 449  
 Mac Low, M.-M., Norman, M.L., König, A., & Wardle, M. 1995, ApJ, 442, 726  
 Marsh, N., & Svensmark, H. 2003, Space Science Reviews, 107, 317  
 Matsumura, S., & Pudritz, R.E. 2003, ApJ, 598, 645  
 Muzerolle, J., et al. 2000, ApJ, 535, 47  
 Najita, J.R., Strom, S.E., & Muzerolle, J. 2007, MNRAS, in press (arXiv:0704.1681)  
 Oppenheimer, M., & Dalgarno, A. 1974, ApJ, 192, 29 (OD74)  
 Pessah, M., Chan, C., & Psaltis, D. 2007, ApJ, submitted (arXiv:0705.0352)  
 Ratzka, Th., et al. 2007, A&A, in press  
 Salyk, C., et al. 2007, ApJL, 655, L105  
 Sano, T., Miyama, S.M., Umebayashi, T., & Nakano, T. 2000, ApJ, 543, 486  
 Sano, T., Inutsuka, S.I., Turner, N.J., & Stone, J.M. 2004, ApJ, 605, 321  
 Spitzer, L. 1978, Physical Processes in the Interstellar Medium, Wiley-Interscience  
 Stelzer, B., & Schmitt, J. H. M. M. 2004, A & A, 418, 687  
 Strom, K., et al. 1990, ApJ, 362, 168  
 Telleschi, A., Guedel, M., Briggs, K.R., Audard, M., & Palla, F. 2007, A&A, in press (astro-ph/0612338)  
 Umebayashi, T., & Nakano, T. 1980, Pub. Astron. Soc. Jap., 32, 405  
 Weidenschilling, S.J. 1977, MNRAS, 180, 57  
 Wolk, S.J., et al. 2005, ApJ, 160, 423